Available online at www.sciencedirect.com

ScienceDirect

Advances in Space Research 62 (2018) 1434–1444

ADVANCES IN SPACE RESEARCH (a COSPAR publication)

www.elsevier.com/locate/asr

Impact of long ocean waves on wave height retrieval from SAR altimetry data

T. Moreau [a,*], N. Tran [a], J. Aublanc [a], C. Tison [b], S. Le Gac [b], F. Boy [b]

[a] *CLS, 11 rue Hermès, Parc Technologique du Canal, 31520 Ramonville St Agne, France*
[b] *CNES, 18 avenue Edouard Belin, 31401 Toulouse Cedex 9, France*

Received 28 February 2017; received in revised form 6 April 2018; accepted 4 June 2018
Available online 12 June 2018

Abstract

SAR altimetry is a new high-resolution operation mode exploited in new-generation altimeter missions, such as Sentinel-3. It takes advantage of its enhanced along-track resolution to make measurements of sea surface height variations in much greater detail than what can be achieved with conventional low resolution instruments (e.g. the Jason-3 altimeter). However, contrary to what is observed for conventional altimetry, long-wavelength ocean waves of a few hundred meters (swell and extreme wind waves) are no longer fully imaged in the instrument ground cells, and SAR waveforms have distorted shapes in such wave conditions. This affects the final retrieval of significant wave height (SWH). This paper analyzes the impact of long ocean waves on SAR-mode data by using both Cryosat-2 measurements and simulated data. Results from these two approaches are in good agreement and show that the estimated parameters from SAR-altimetry waveforms are particularly noisy under long-wave conditions and also biased when compared with conventional altimetry data. Additionally, we found evidence that these impacts are different between the two directions (along and cross-track directions) due to the asymmetry of the SAR-altimetry footprint. Simulations indicate that statistics of sea surface elevations within the SAR-altimetry footprint deviate from Gaussian behavior. The assumption commonly used for ocean retracking algorithms is therefore inaccurate. The sensitivity of SAR-mode altimetry data to long waves is a key issue for the ocean altimetry community, which is concerned to ensure the continuity of high-quality time series of the global sea-surface topography in future years. This is not only an issue for these new-generation radar altimeters (Sentinel-3 and Sentinel-6) but also for all innovative techniques or processing methodologies capable of providing higher spatial resolution of the ocean surface.

Keywords: SAR altimetry; Significant wave height; Impact; Sea state; Long ocean waves

1. Introduction

Ocean surfaces are regularly probed by radar altimeters that provide spatial distribution of sea surface height along with significant wave height (SWH) and wind speed. The launch of the Cryosat-2 satellite in 2010 opens a new era in the way we observe the oceans with a new generation of altimeters operating in the so-called Synthetic Aperture Radar (SAR) or Delay-Doppler altimetry mode. They do not work in a pulse-limited mode (referred to as the low resolution mode: LRM) like conventional radar altimeters but use an innovative processing technique that aims to improve measurement quality. A first-stage processing combines coherently the returns from many pulses to increase the radar resolution in the along-track dimension, then an incoherent summation processing enhances the signal-to-noise ratio (Raney, 1998; Wingham et al., 2006).

By reducing the antenna footprint along the satellite track from 12 km in LRM to 300 m in SAR altimetry mode (for Cryosat-2), the illuminated area on the sea surface has now a size similar to or smaller than some of the long ocean

* Corresponding author.
E-mail address: tmoreau@cls.fr (T. Moreau).

https://doi.org/10.1016/j.asr.2018.06.004

wind waves and swell (i.e. waves of a few hundred of meters in length up to 600–700 m for the longest ones which occasionally occur away from the most severe storms (Sterl and Caires, 2005)). As a consequence of this narrowing view, SAR altimeter may see only a portion of the long-waves period, which induces variations on the illuminated radar footprint and on the surface height distribution inside this footprint. These effects are expected to further influence the shape of the measured waveforms, depending on which portion of the long-wavelength wave is imaged. We can even anticipate that this distortion would become more severe as the mean wave period and wave height of the wave system increase. Furthermore, it is also expected that the surface elevations within the surface footprint differ from a Gaussian distribution. This would cause errors in SAR altimeter geophysical retrievals from any retracking model relying upon Gaussian sea surface elevation statistics (Halimi et al., 2014; Ray et al., 2015; Boy et al., 2017). All these open issues about the accuracies of the SAR retrieved parameters have to be tackled to ensure a good continuity of altimetry measurements from SAR mode data with respect to past LRM mode data.

In this paper, we present an analysis of the impact of long ocean waves on high-resolution SAR mode measurements by focusing in particular on the wave height retrieved parameter, which seems at first order the primary affected parameter. This was done by comparing measured data from the Cryosat-2 mission with estimates from a wave model. Simulated data were then generated to confirm the observations obtained. Section 2 provides an overview of the SAR processing and a discussion of the assumptions used in the retrieval algorithm. Section 3 presents the analysis performed based on the Cryosat-2 data, while Section 4 provides results from the simulation analysis. Finally, the key findings are discussed in the Conclusion.

2. SAR altimetry overview

Cryosat-2 is a European Space Agency (ESA) Earth Explorer satellite carrying the first radar altimeter able to operate in the innovative high-resolution SAR mode (Wingham et al., 2006). This is known as SIRAL, a contraction of Synthetic Aperture Radar and Interferometric Radar Altimeter, and can also operate in two other modes: namely Low Resolution Mode (LRM) and SAR Interferometry (SARIn) mode. Primarily dedicated to precise monitoring of ice-covered land and sea surfaces, it also performs experimental data acquisition over oceans, thereby providing the first opportunity to evaluate the performance of SAR altimetric data under such conditions. Though the amount of ocean data to analyze is rather limited, due to the restricted number of areas probed in SAR mode, several reported analyses have highlighted its capability to also provide valuable data over the ocean. The sea-surface topography is observed more precisely and in much greater detail than with conventional radar altimeters, thanks to specific data processing (Gommenginger et al., 2013; Cotton et al., 2015; Fenoglio-Marc et al., 2015; Boy et al., 2017; Raynal et al., 2018). Indeed, SAR altimeters should theoretically enable us to map sea surface height structures down to sub-mesoscale (around 10 km) (Raynal et al., 2018), where conventional altimetry observations are inaccurate due to some correlated observation errors (hump artifacts) observed for scales smaller than 100 km (Dibarboure et al., 2014).

2.1. Processing principle

In SAR mode, the altimeter transmits pulses in bursts of 64 pulses at a high Pulse Repetition Frequency (PRF) of approximately 18 kHz. Such a PRF is about ten times higher than that used in LRM mode, and inherently ensures a high level of phase coherence from pulse to pulse within the burst. Correlated groups of returning echoes are then handled in a two-step process summarized briefly: (1) unfocused coherent processing is performed over a sequence of radar returns to synthesize a set of relatively narrow beams that point in different directions (or look angles) along the ground track of the satellite; then (2) an incoherent averaging of multiple and independent looks of the same ground scene is applied to reduce the speckle noise. More details can be found in the papers of Raney (1998), Wingham et al. (2006) and Boy et al. (2017). The SAR-altimeter measurement principle will also be discussed in Section 4 in relation to the simulation of SAR waveforms.

In contrast with conventional altimetry, the area illuminated at 20-Hz after the coherence processing is not a surface-constant ring (in red in Fig. 1), but a surface delimited by thin strips along the satellite track, as illustrated in Fig. 1. Delay-Doppler radar then looks at a smaller section than the pulse-limited radar footprint. For Cryosat-2 SAR first resolution cell, the along-track resolution is ∼300 m

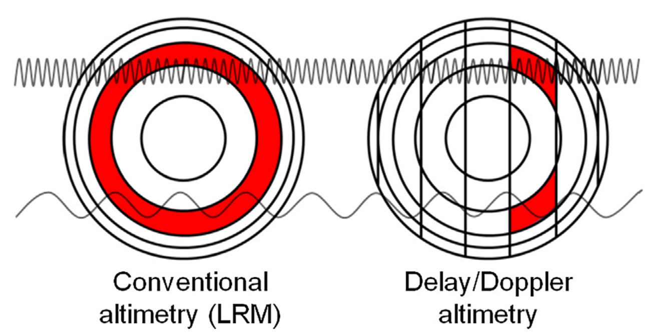

Fig. 1. Sketch of the footprint geometry for conventional (left panel) and delay/Doppler (right panel) altimetry. Only a few range rings and Doppler lines are drawn in the figure for clarity reasons, but around 80 samples are used in distance and 64 Doppler beams are synthesized for each processed burst from SIRAL. One measurement cell is colored in red for both radar modes, and a short and a long wavelength wave are superimposed. (For interpretation of the references to colour in this figure legend, the reader is referred to the web version of this article.)

while the across-track resolution is ~800 m, like the radius of the LRM cell. Therefore, each consecutive 20-Hz strip does not overlap nearby ones, making SAR-mode measurements free of correlated observation errors leading to hump artifacts on sea level anomaly power spectra, which on the contrary affect LRM data for scales smaller than 100 km (Dibarboure et al., 2014).

Pulses acquired in SAR mode can also be used to generate low-resolution data (so-called pseudo- LRM data) similar to those produced by conventional altimeters to help in the validation of this new functioning mode. The PLRM or "reduced SAR" echoes are created by grouping and summing the SAR mode echoes into LRM-like power waveforms, which are then processed as LRM waveforms. However, since a lower number of incoherent echo pulses (32 as against 90) is averaged in a 20-Hz radar cycle, PLRM measurements are noisier than LRM ones.

2.2. Geophysical retrieval algorithm

The retrieval of ocean parameters (sea level, significant wave height and wind speed) by a retracking process is achieved by fitting the return echo with an analytical model. For conventional altimetry, the Hayne model (1980) or the Amarouche model (2004) are usually considered. They are based on the original formulation given by Brown (1977), which assumed that the ocean waves on the sea surface come from a linear system driven by Gaussian statistics of heights and slopes. Later models take into account higher order moments of the ocean wave elevation distribution to better characterize the (weakly) nonlinear nature of ocean waves. Typically, a wave skewness value fixed at −0.1 is used. In association to this echo model, a so-called "unweighted Least Square Estimate" derived from a Maximum Likelihood Estimator (MLE) (Dumont, 1985; Rodriguez, 1988) is implemented in most altimeter ground processing chains.

Cryosat-2 PLRM data are processed with an ocean retracker equivalent to the so-called MLE4 algorithm for Jason-2, where the measured waveform is fitted with a 4-parameter return power model. The four parameters in MLE4 are waveform delay (related to range), waveform amplitude (related to sigma0, hence to wind speed), waveform rise time (related to SWH), and antenna mispointing.

For SAR altimetry, various ocean models (Halimi et al., 2014; Ray et al., 2015; Boy et al., 2017) have been developed recently, using the same practical assumptions used by Brown (1977) and Hayne (1980) in their models for sea-surface description (i.e. a Gaussian-shaped probability distribution of the surface elevations and slopes). This assumption stands for the case where the topography of the open ocean surfaces is homogeneous within the altimeter footprint. This applies for conventional LRM altimetry because of its large ground resolution cells (of ~4 km^2 for Jason-2 and ~2 km^2 for Cryosat-2 PLRM). It is now questionable, when one considers SAR strip-shaped footprints of smaller size (~0.5 km^2) and when waves of close or larger wavelength than the along-track strip size (a few hundred meters) dominate the observed sea state. In such cases, only a portion of the wave profile would be seen in the footprint.

Therefore we are concerned that ocean wind waves with long wavelengths (>300 m) affect the shape of the SAR-processed waveforms in approximately the same way as continental topography affects the shape of the LRM waveforms recorded over undulating surfaces (Berry et al., 1997; Legresy and Remy, 1997; Arthern et al., 2001). We can even anticipate that this distortion would become more severe as the wavelength and wave height of the wave system increase.

Moreover, since the SAR footprint does not have the isotropic character of the LRM footprint, potential impacts on SAR waveforms of differential propagation direction of the waves with respect to the radar's along-track direction has also to be considered along with their wavelength values.

It is therefore of great interest to examine how the shape and intensity of the SAR-altimeter waveforms are affected by wave systems encompassing long-wavelength ocean wind waves, and whether they differ from the shape of the ocean model used in the retracking algorithm. Any deviation from Brown's assumptions would cause errors in SAR altimeter retrieval of geophysical parameters based on any retracker model relying upon Gaussian sea surface elevation statistics (Halimi et al., 2014; Ray et al., 2015; Boy et al., 2017).

With the availability of the Cryosat-2 data, we propose to evaluate the impacts of long ocean waves characterized by both their wavelength and propagation direction on SAR altimeter-derived parameters. This could provide helpful insights for the choice or the definition of processing algorithms for the newly launched Sentinel-3A and the follow-on units, and in the preparation of the future Sentinel-6 topography missions which each embark a SAR altimeter.

Impact on SAR range retrieval is already expected since it has been shown by Tran et al. (2010b) that for LRM missions, taking into account the mean wave period (denoted T02) in the sea state bias correction significantly improves sea level accuracy. Solutions for handling such effects on range already exist. The big unknown so far is the impact on SAR significant wave height estimates that has not been documented in published literature. This paper will focus primarily on the SAR SWH estimates by comparing them with PLRM and wave model data. Some results will be reported about SAR range while analysis of SAR backscatter cross-section is outside the scope of this paper.

3. Analysis of Cryosat-2 data with collocated WW3 data

3.1. Datasets

The Cryosat-2 data used in this analysis are provided by the CNES ground segment Cryosat-2 processing prototype

(CPP), which routinely processes LRM and SAR mode data from ESA raw data (Boy et al., 2017). Official ESA products were not used because the Cryosat-2 ground segment chain does not provide SAR data at this time, because full processing is not completely implemented. One difference between the two processors lies in the way they compute the surface sample location. The CPP enables PLRM and SAR mode data to be derived from the same echoes so that direct cross-comparisons can be made.

The Cryosat-2 data are from cycles 68 to 75 (i.e. 09/05/2015 to 26/12/2015) corresponding to about a half-year period. Since the coverage of Cryosat-2 observations in SAR mode is not global but from a limited number of geographical areas (patches), we did use some LRM data from Jason-2 altimeter to test whether the Cryosat-2 SAR-mode patches are sufficiently representative of global wave systems. Jason-2 measurements from cycles 254 to 273 (i.e. 25/05/2015 to 10/12/2015) were used.

These altimeter data have been collocated with WaveWatch-III (WW3) numerical model grids in space and time at the altimeter ground track locations to get external information about ocean surface waves. The WW3 grids correspond to IFREMER version products obtained from ftp://ftp.ifremer.fr/ifremer/ww3/HINDCAST/GLOBAL/2015_ECMWF. They are provided as a global 0.5° × 0.5° wave grid from 78°S to 80°N at 3-h time steps. The model run was forced by ECMWF winds. More information on the WW3 model can be found in Rascle and Ardhuin (2013).

3.2. Wave systems climate

The significant wave height (SWH or Hs), the mean wave period (T02) and the mean wave direction (Dir) are the most common parameters used to characterize sea states. They are provided by the WW3 wave model. Therefore, instead of using wavelength (L) values in what follows we will analyze the data with respect to T02 estimates. They are computed as the square root of the ratio of m0 to m2 where m0 and m2 are the zero-order and the second order moments of wave field statistics. For deep water conditions reflecting the prevailing conditions over most of the ocean areas, the relationship between these two parameters is $L \sim 1.6^{*} (T02)^2$. A criticism concerning the use of these parameters could be that they provide a limited description of the wave field, since they are calculated by integrating the wave spectrum. Indeed, a mixed sea state of wind-sea and swell waves can have the same SWH and Tm as a slightly higher wind-sea without swell (Semedo et al., 2011).

Thanks to a spectral partitioning technique, the WW3 model may separate wind-sea and swells from mixed waves and provide information for each of the wave systems: wave height, wave peak period and wave direction for the wind-sea system along with those for each of the three swell systems. It should be mentioned that, with regard to the swell systems, the first swell component (called swell#1) is the largest swell wave, the next (swell#2) is the second largest swell wave, and so on.

Fig. 2 shows a histogram of WW3 SWH for each of the wave systems from the Jason-2 collocated dataset. As can be seen in this figure, wave height up to 6 m can exist for both wind-sea and swell#1 waves. Heights for swell#2 and swell#3 are always lower than 2 m for cases of mixed seas with different swells. The peak location for wind-sea is located at approximately 1.8 m. For swell waves, this value is lower and decreases as we go from swell#1 to swell#3. Comparable plots (not shown) have been obtained from Cryosat-2 SAR-mode patches compared to those observed on global ocean coverage as provided with the Jason-2 altimeter.

A closer look at the data reveals that the global wave field consists generally of mixed sea with swell. Among the different wave systems observed with the global coverage between 50°N and 50°S latitude, only 3% of the dataset corresponds to pure wind-sea situations. For 40% of the cases, the wave fields are composed of only swell waves without wind waves. Regarding the geographical distributions of occurrences, we also notice that the global wave field is dominated by swell everywhere, even within extratropical storm areas where the relative weight of the wind-sea part of the wave spectra is the highest. Occurrences of swell systems are close to 100% in the tropical band (Chen et al., 2002).

In Fig. 3, swell waves generally display longer peak period values than wind-sea waves, with some overlap for period values between 6 and 12 s. However, the mean wave period is closer to the wind-sea peak period. This is expected, since several wave systems with distinct characteristics (different wavelengths, wave heights and propagation directions) contribute to the total sea state at most

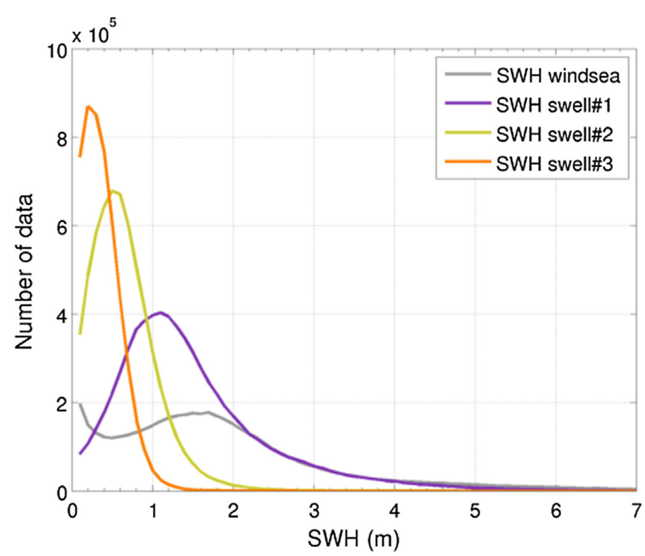

Fig. 2. Histogram of WW3 SWH for each of the wave systems from the Jason-2 dataset (data from 25/05/2015 to 10/12/2015 with global coverage of the ocean).

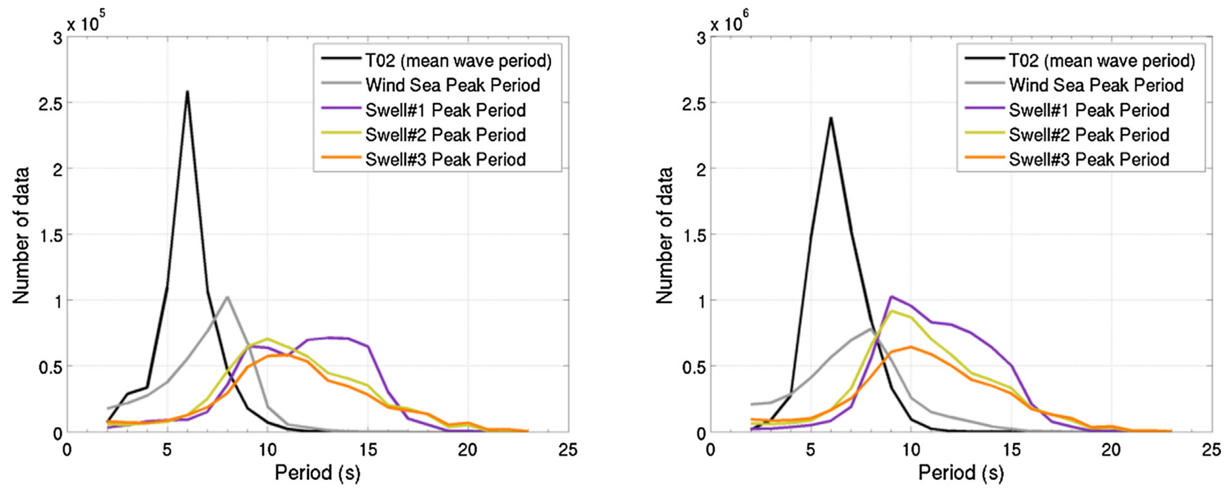

Fig. 3. Histograms of wave period (mean values: T02 or peak values for each wave system) for the Cryosat-2 subset (left) and the Jason-2 subset (right).

locations. It seems thus more interesting to use mean values for the wave characteristics for the present analysis of the SAR data instead of those for the different swell systems, since the radar sees a chaotic ocean surface within its footprint.

Besides the wave height and period, a sea state is also characterized by its propagation direction. In this regard and as a common oceanographic practice, it is worth recalling that the swell direction is measured positive clockwise from due north. Thus a swell coming from due north (and therefore heading south) is said to be coming from 0°; a swell coming from due east (i.e. heading west) is said to be coming from 90°; and so on. Concerning the propagation direction of the wave systems collocated with Jason-2 altimetry observations (Figures not shown), we observed some prevailing orientations for wind-sea and swell#1 and larger variability for swell#2 and swell#3. For instance, concerning swell in the Pacific, north-east trade winds generate a north-east swell, and the south-east trade winds create a south-east swell. Storms in the South Pacific during austral winter generate a south swell, and storms in the North Pacific generate a north swell.

From this comparison, we see that the Cryosat-2 SAR-mode patches are representative of the global ocean in terms of wave systems because we have very similar distributions to those from Jason-2 data. The only downside is that this dataset involves a small number of samples to describe the data behavior in the 3-dimensional space (SWH, T02, Dir); hopefully, some statistically stable features will nevertheless be highlighted within the dense data area to provide some insights on how to analyze the newly acquired Sentinel-3 data.

3.3. Analysis of SAR SWH data with respect to wave characteristics

Cryosat-2 SWH differences between the SAR and PLRM estimations are presented in Fig. 4 for different T02 and SWH values. Clear features are highlighted. The differences depend on both SWH and T02 within two regime-types. For small SWH values (<1.5 m), the difference increases as the SWH values go up but variations with T02 can be neglected. Above 1.5 m of SWH, the difference increases more slowly with SWH but variations with T02 are clearly visible. Differences with T02 may differ by as much as 5–10 cm for a given SWH value, and certainly even more for longer waves. Biases between SAR and PLRM estimates vary, therefore, according the sea-state parameters. All of this leads us to conclude that the measurement accuracy is not the same for these two modes.

Fig. 5 indicates that the standard deviation (STD) of the 20-Hz SWH measurements (also called "noise") depends on both SWH and T02 for the two processing modes with, however, a much smaller effect on PLRM. In the case of the SAR mode, we observe a larger variation with respect to T02 (and SWH for high T02). This result was confirmed

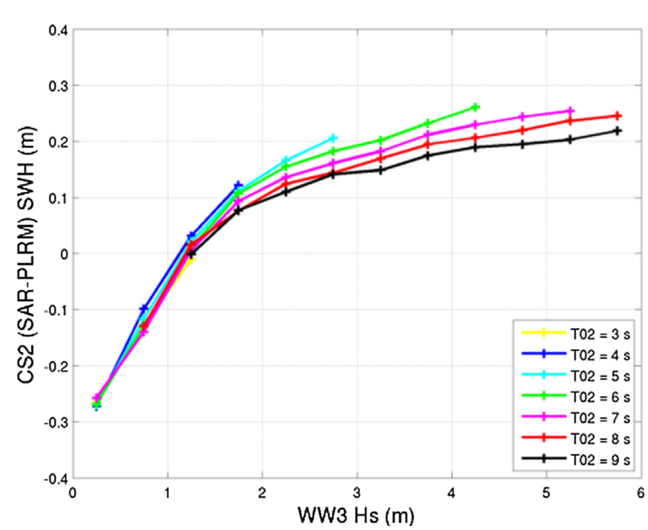

Fig. 4. Bin-averaged values of Cryosat-2 (SAR minus PLRM) SWH against WW3 SWH estimates for seven different T02 values.

through along-track MQE (mean quadratic error) analysis, which showed higher levels of MQE for larger T02 values in the case of SAR-mode data, while in the case of PLRM the level of MQE is fairly constant. Note that the MQE quantifies the misfit of the model waveform found by retracking algorithms.

The STD of the 20-Hz SWH measurements shown in Fig. 5 is now plotted against the wave propagation angle with respect to the satellite flight direction (also called relative azimuth direction) in Fig. 6. The relative azimuth direction is defined as the difference between the WW3 mean wave direction and the satellite along-track heading direction, with both directions referenced with respect to true North. From this Figure, one can observe that STD of the 20-Hz SAR SWH data does not only depend on SWH and T02, but also on the relative azimuth direction, as evidenced by this small but clear wave direction signal up to 7 cm peak-to-trough. Furthermore, we observe higher STD of the measurements when waves propagate parallel to satellite ground track displacement than when the two directions are perpendicular. This is observed for SAR data because of the asymmetric shape of the SAR altimeter footprint. On the other hand, as expected, no angular effect is observed on PLRM measurement STD, since the ground footprint of conventional altimeters is circularly symmetric. These results will be confirmed with the simulations performed in the next section.

In view of the behavior displayed in Fig. 6, this relative azimuth direction (z) dependence can be empirically modeled by a second-order Fourier series of the form: a0 + a1 cos(z) + a2 cos(2z), where a0, a1 and a2 are regression parameters. To describe more precisely this azimuthal variation with respect to SWH and T02, we will need to analyze the behavior of the regression parameters, which cannot be found using the small Cryosat-2 SAR dataset used here. Future analysis of data from the newly launched Sentinel-3A, which provides global ocean sampling, would give us further insights to describe this behavior.

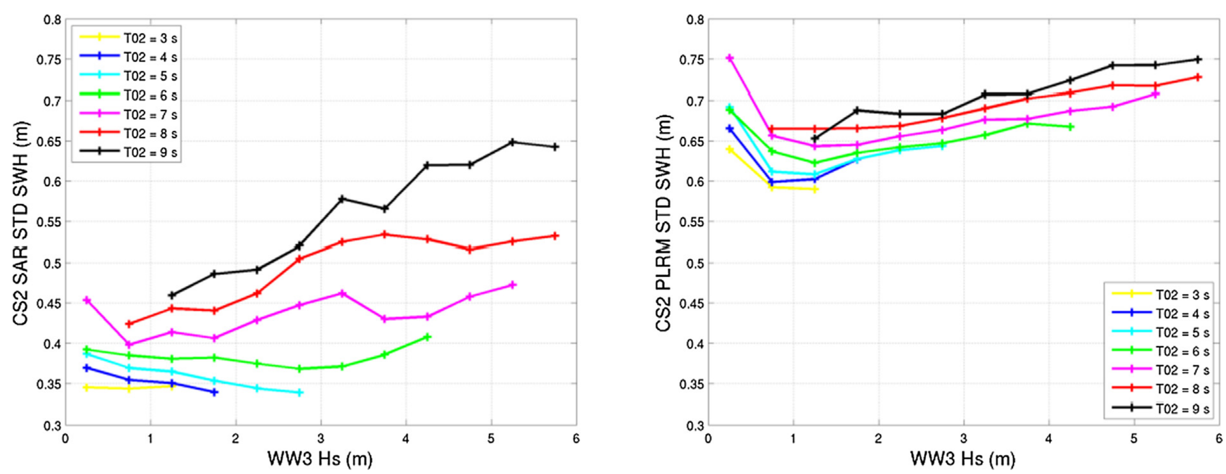

Fig. 5. STD of 20-Hz Cryosat-2 SAR (left) and PLRM (right) SWH against WW3 SWH estimates for seven different T02 values.

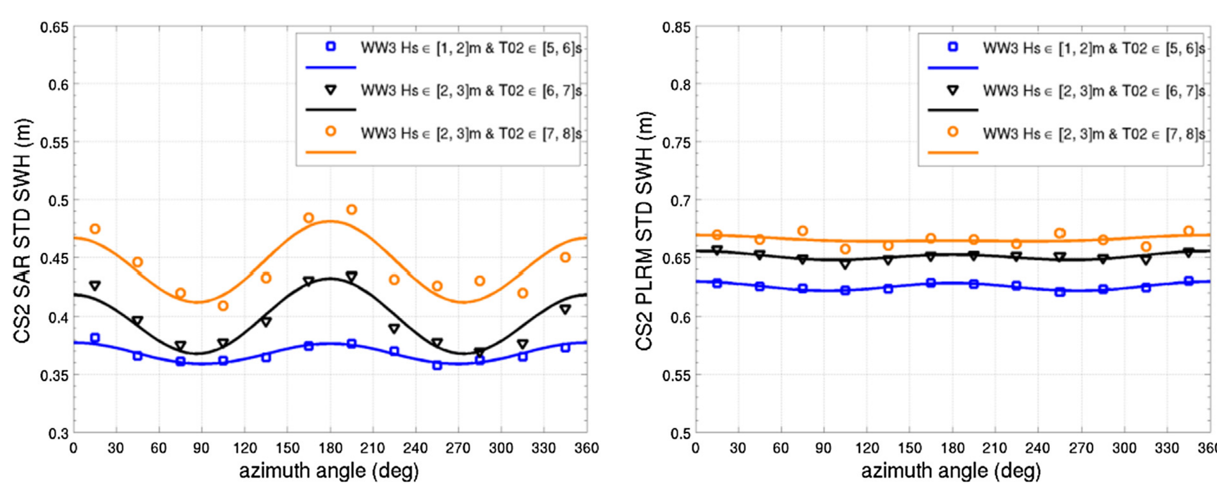

Fig. 6. Wave direction signal (with respect to satellite flight direction) in 30° bins of STD of 20-Hz SWH in (left) SAR and (right) PLRM modes for different SWH and T02 values. The solid line represents a second-order harmonic fit.

4. Waveform simulation and retracked SWH values

4.1. Simulation approach

Simulations were conducted to better understand the results of the analysis done with Cryosat-2 SAR data. Two objectives were pursued: first to confirm the behavior observed in real data and secondly to further characterize the effects of wave characteristics on the high-resolution SAR data. For this, an in-house simulator with an end-to-end simulation capability was developed and adapted to Cryosat-2 SIRAL specifications. It consists of three main successive simulation modules corresponding to the sea surface, the on-board processing and the ground processing, respectively. The end-to-end simulator is close to the one developed by Boy et al. (2017). Unlike the latter, however, it is capable of generating entire SAR data stacks over a simulated sea surface of any wave condition, making it a highly versatile and useful tool for investigating sea-state effects on low- and high-resolution mode altimetric data.

The simulator incorporates a number of existing wave spectrum models, enabling users to generate realistic sea surfaces (based on a Fourier domain approach) for any combination of swell (Durden and Vesecky, 1985) and wind-sea conditions. An example of surface realization is shown in Fig. 7. The simulated sea surfaces are rectangular grids of about 20 km wide (10 km on either side of the flight track) and 13 km in the along-track direction (azimuth). They are far larger than the radar footprint of the SAR altimeter waveform, and long enough in the azimuth direction to allow the generation of about forty consecutive waveforms sampled at a rate of 20 s^{-1} along the orbit. This is of particular interest when one examines the STD of the altimeter estimates along a track crossing ocean swell features. A total of 6700×4300 grid points resulting from the discretization of the simulated surface with a 3-m resolution (which is very small compared to the cross-track and along-track resolution of the SAR radar altimeter) are processed for each simulation run.

Fig. 7 illustrates schematically the simulation principle for the generation of the SAR-mode waveforms. Briefly, for each position of the satellite in its orbit, a single look echo waveform is computed as the sum of the backscattered powers recorded by each radar range gate of the waveform. For this, each grid point contribution is weighted by the antenna gain pattern considering the local slope of the surface. Then a set of single look waveforms generated from different look angles is gathered at the same surface sample, to form a stack. They are then corrected in range to align each other with respect to the nadir position, and finally averaged to create the SAR altimeter waveform (or multi-look waveform).

Due to numerical efficiency constraints and weak effects on computed SAR waveform shape, we simplified the

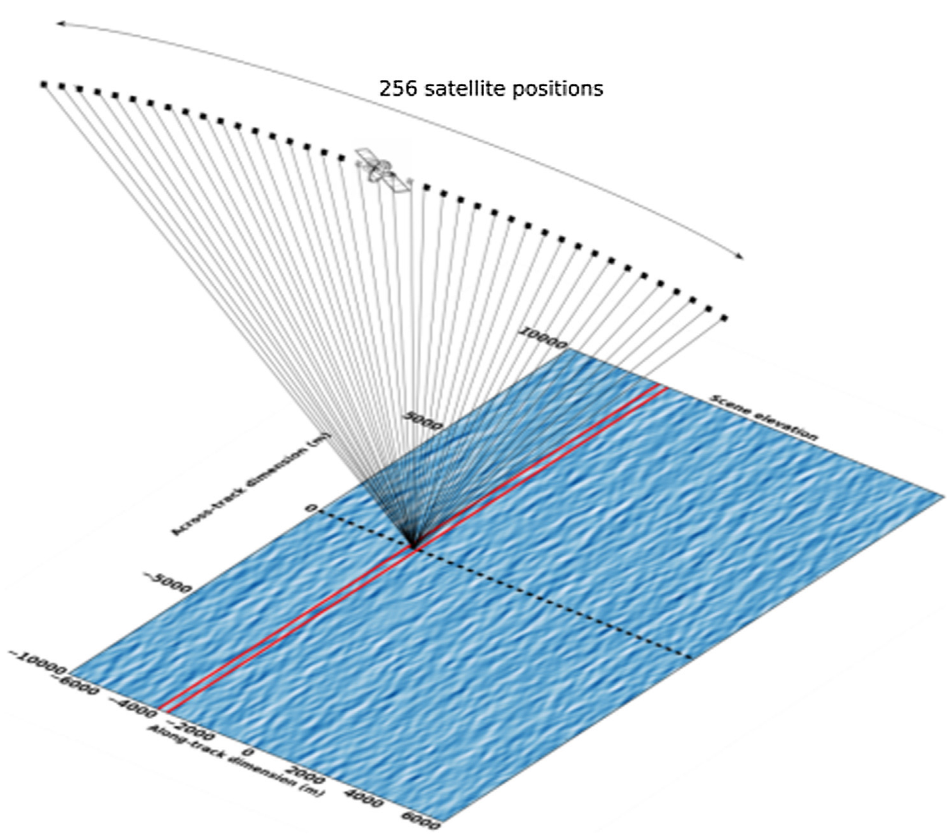

Fig. 7. Scheme of the Cryosat-2 multi-look process in SAR mode as implemented in our simulator. Multiple synthesized looks seeing the same 300-m-width strip are combined to create a multi-look waveform.

waveform generation by neglecting the along-track point target response (PTR) and its multiple side lobes in the numerical integration. This assumption is perfectly acceptable as long as the waveform model used in the retracking algorithm is consistent with this choice.

4.2. Sea-state effects on simulated SAR-mode data

To simplify the analysis of the sea-state effects and make it more comprehensible, pure swells with waves from one direction were considered in this study, even though mixed seas (composed of wind-sea and swell systems) are prevalent in the world oceans. Swell fields present a reduced amount of randomness when one compares them with pure wind-sea fields, and form orderly undulations of the ocean surface with more defined shape and direction. In so doing, changes in simulated SAR waveforms could be directly correlated with sea-state parameters (i.e. wave height, wavelength and wave propagation direction) and the impact of each parameter on SAR SWH estimates would be more easily assessed.

Fig. 8 presents a simulated stack (on the left panel) and multi-look waveforms (on the right panel) for different swell conditions (SWH = 3 m and peak wavelengths L = 400 m and L = 600 m) and a sea case with non-undulating surface (i.e. as it is assumed for waveform retracking). From this Figure, there are clear indications that the waveform shape is altered by waves of long wavelength (i.e. distorted leading edge and undulations in the decreasing tail of the waveform), whereas the waveform has a relatively smooth shape over sea surface waves of short wavelengths. Additionally, it can be said that the changes in waveform shape are more pronounced for the longest wavelengths (L = 600 m), highlighting concerns about the waveform retracking to accurately estimate the parameters with the fitting process.

Different swell scenarios were simulated by varying parameter values in the model: three wave height values were used (3, 5, 7 m), five wavelengths (100, 200, 300, 400, 600 m), and three wave propagation directions with respect to the satellite track (i.e. azimuth angles of 0, 45, 90°). For each scenario, 660 waveforms were generated and both SAR- and PLRM-mode SWH estimates were derived from each waveform. It is also important to emphasize that the statistical properties of the sea-surface heights and slopes follow Gaussian distribution at the scale of the surface simulated patch (larger than swell wavelengths used in the model).

Fig. 9 illustrates the 20-Hz bias (i.e. with respect to the sea-state parameter used in simulation) and noise for SWH estimates for the different swell conditions used in our simulations. While the three azimuth angles are considered for the SAR retrieved values, only one angle was provided for the PLRM values (i.e. azimuth angle of 0°) due to the symmetrical character of the footprint. As expected for the PLRM data, there is a negligible variation of the bias and no variation of the noise level with respect to the swell wavelength. A clear dependence is observed between the 20-Hz noise of the SAR-altimeter estimates and the swell parameters (wavelength and direction of propagation). Same effects are observed for larger wave heights but not shown here. The highest values of 20-Hz bias and noise are obtained when waves of wavelength larger than 300 m are traveling in a direction parallel to the satellite track and they increase as the wavelength goes up. Variations observed in the bias values indicate that the accuracy of the SAR SWH is impacted differently according to the wave field conditions. This confirms results reported above from the Cryosat-2 SAR data. Note that the bias and noise values observed on the simulated data and from the Cryosat-2 data cannot be directly compared for two different reasons. On one hand the speckle and thermal noise are

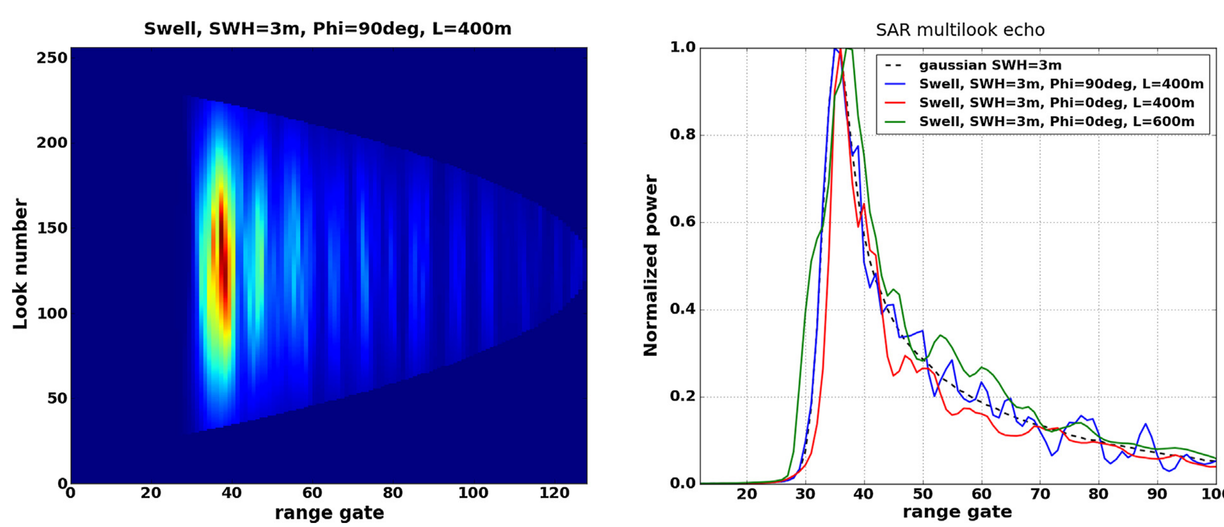

Fig. 8. Simulated stack of collocated looks (left) and SAR-altimeter waveforms (right) as calculated over a well-developed ocean swell (SWH = 3 m, L = 400 m, and two directions of wave propagation with respect to the sub-satellite track). A waveform obtained for a longer wavelength (L = 600 m) is added for comparison.

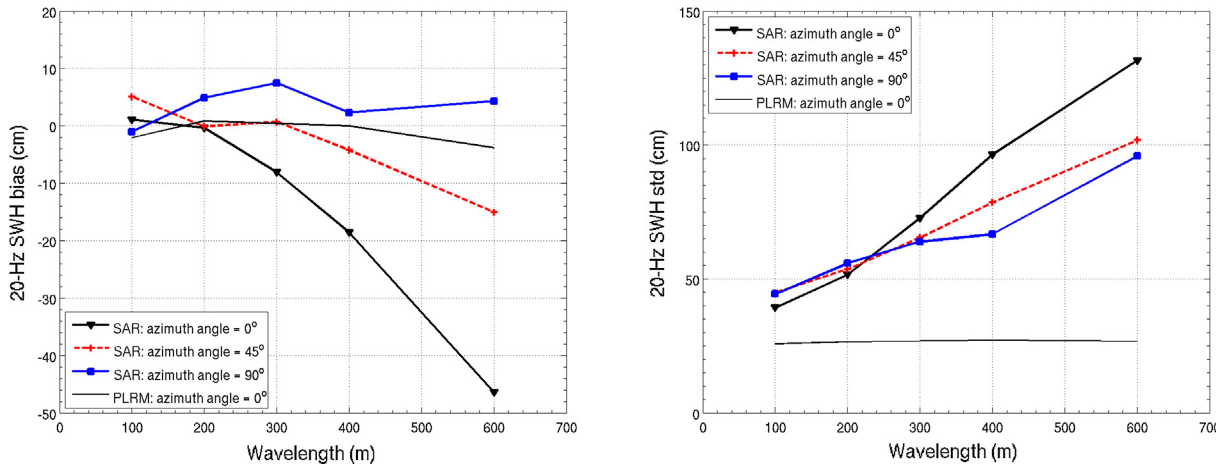

Fig. 9. Computed 20-Hz bias and noise for SWH as a function of both swell wavelength and azimuth angle for SWH = 3 m. The SWH values have been computed for both the SAR and the PLRM modes.

not accounted for in our simulations and on the other hand, pure swell fields were not found with enough occurrences in the collocated Cryosat-2/WW3 dataset to describe stable statistical behavior. Note that for real data, our analysis does not use the peak wave period but the mean wave period because of the mixed sea conditions predominantly imaged by the radar. However, these two analyses both highlight the same type of change in SAR retrieved SWH depending on the characteristics of the long ocean waves.

One of the key factors determining the accuracy of the retrieved SWH value is the correct description of the probability density function of the sea surface elevations in the waveform model. This function is commonly assumed to be Gaussian in the ocean models currently used for SAR-altimeter data processing. However, this assumption is no longer valid in long-swell conditions. Fig. 10 provides a simple illustration of why this tends to be so. In this figure, the distributions of the scatterer elevations within a SAR-altimeter resolution cell (300 m × 2 km) are computed for swells of various wavelengths (L = 0, 25, 200 and 600 m), and for two different locations of the cell on the sea surface (corresponding to left and right panels in Fig. 10, respectively). We can see that the statistical properties of the scatterer elevations within a SAR-altimeter resolution cell lose their Gaussian character as the dominant wavelength of the ocean waves becomes greater than this cell size, even if the distribution of the simulated surface height and slope are Gaussian. Besides, the distribution of the sea surface elevations is not repeatable from one location to another one in long-swell conditions. The distortion of the waveform shape leads to degradation in the altimeter estimates because of the improper use of a retracker model relying upon Gaussian sea surface elevation statistics. Under ideal sea conditions (referred to as L = 0 m in Fig. 10), the distribution of the scatterer elevations within that resolution cell is perfectly Gaussian.

Although the simulation results confirm the general trends arising from Cryosat-2 data, some remaining discrepancies are observed, which we believe may be caused by the neglect of the sea surface height displacement during the acquisition of all stacked looks in the multi-looking

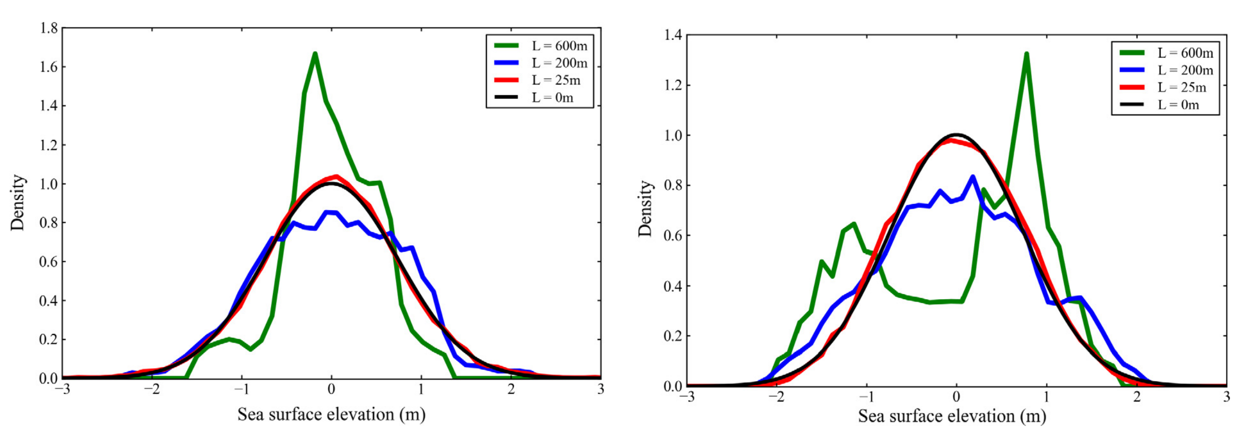

Fig. 10. Examples of sea surface height distribution computed within a 0.3 km × 2 km resolution cell for swell cases of different wavelengths. The Gaussian reference is obtained for L = 0 m. Left and right panels correspond to two different locations of the resolution cell on the surface.

process (~2.5 s). Simulations based on a static sea surface were preferred, to allow quantitative statistical analysis. However, this approach deals poorly with the dynamical properties of the ocean surface that may be of particular importance in SAR altimetry in addition to the loss of gaussianity within the resolution cell. The surface movement is a key issue for efficient simulation. This is still a subject to be tackled.

Furthermore, it may be pointed out that the occurrence of swell with a wavelength of more than ~600 m is not very common in nature. This particular swell condition was only considered in our simulation to demonstrate that the distortion of the sea surface height distribution becomes more pronounced with the wavelength of the wave system.

5. Conclusions and perspectives

SWH measurements are operationally used together with wind speed estimates to correct altimeter sea surface height measurements for sea state related biases. In this study, we attempt to analyze the sensitivity of the SWH data from the new SAR-altimeter operating mode to long ocean waves characterized by wavelengths of the same order of magnitude as the SAR-altimeter along-track resolution (a few hundred meters).

We first compared eight months of Cryosat-2 data obtained with the two operating modes (SAR- and PLRM-mode), to highlight their differences in terms of sea-state dependencies by using collocated WW3 data. Results showed that in terms of bias, the SWH differences between the two modes depend both on the values of WW3 SWH and T02, thus revealing potential inaccuracies in the SWH retrieval for SAR-mode (when compared with PLRM). Furthermore, it was found that the 20-Hz SAR SWH noise is highly dependent on both SWH and T02 but also exhibits a distinct wave direction related signal with respect to the satellite flight direction (higher STD of the measurements is observed when waves propagate parallel to satellite ground track displacement). Since SWH and range data are output from the same processing algorithm, we also paid some attention to evaluating the range differences between the two radar modes. While the analysis is not yet completed, preliminary results indicates that the range differences do not depend on T02. This suggests that the challenges to compute SAR mode sea state bias (SSB) correction for SAR-altimeter ranges are the same than for conventional LRM-altimetry. Standard empirical approaches to develop the SSB model are applicable and appear to offer the best way forward (Gaspar et al., 1998, 2002; Labroue et al., 2004; Tran et al., 2010a, 2010b).

Complementary to this Cryosat-2 data analysis, an investigation of the long-wave effects, based on simulated data, was conducted, confirming the different behavior observed. The simulation further suggested that the assumption of a Gaussian distribution of the sea surface elevations used within the ocean retracker model is not always appropriate to describe the statistical properties of the measured scatterer elevations within the SAR-altimeter ground cells. The divergence from Gaussian behavior gets larger with the increase of the mean wave period of the surface waves within the SAR footprint. In cases for which the Gaussian assumption is no longer met, the altimeter waveforms display distorted shapes that cannot be correctly handled by the ocean retracker model. This leads to non-negligible errors in the estimation of the different parameters similar to some reported anomalies observed in conventional altimetry (Tournadre et al., 2006; Thibaut et al., 2010) and increases the standard deviation values of the 20-Hz estimates.

The reported results provide the first evidence of a sea-state effect on altimeter SAR-mode SWH estimations. These results raise further concerns about the potential impact of such ocean wave effects on the sea level time-series when data from the different Sentinel-3 topography missions and the future Sentinel-6 mission, which all have SAR-mode radar altimeter, will be incorporated. Many discussions have taken place to date regarding this issue, and continue to be debated in the altimetry community. Everyone is agreed on the need to extend the analysis to a much larger set of data than is presently available (due to the limited geographic distribution of the Cryosat-2 SAR acquisitions), so that a more complete quantification of these effects on both SWH and range estimates can be carried out. The newly-launched Sentinel-3A mission, which is being operated in SAR mode over the entire ocean, should be able to address this issue in more detail. Further progress in the characterization of these long ocean wave effects is also expected with the upcoming launch of the second satellite of the Sentinel-3 program (Sentinel-3B), planned for the beginning of 2018, and its flight formation with Sentinel-3A.

Given the limitations in the actual SAR-altimeter processing to cope with measurements of long ocean waves, significant concerns are raised about the ocean wave sensitivity of new techniques (e.g. the SWOT high-resolution altimeter) or processing methodologies capable of providing higher spatial resolution, which may dramatically increase the long-wavelength wave effects.

Acknowledgments

This work was supported by the French Space Agency (CNES). The authors are grateful to ESA's CryoSat mission manager, Tommaso Parinello, for sharing SIRAL data. They also wish to thank Laiba Amarouche and Romain Husson from CLS, Alexis Mouche from IFREMER and Lotfi Aouf from Météo-France for the productive discussions held over the course of this project. They would like to acknowledge the indispensable provision of the IFREMER WW3 products by Fabrice Ardhuin to support this study. Finally, this study would not have been possible without the active participation of Nicolas Picot from CNES at the early stage of this research work.

References

Amarouche, L., Thibaut, P., Zanife, O.Z., Dumont, J.-P., Vincent, P., Steunou, N., 2004. Improving the Jason1 ground retracking to better account for attitude effects. Mar. Geod. 27 (1–2), 171–197.

Arthern, R.J., Wingham, D.J., Ridout, A.L., 2001. Controls on ERS altimeter measurements over ice sheets: footprint-scale topography, backscatter fluctuations, and the dependence of microwave penetration depth on satellite orientation. J. Geophys. Res. 106 (D24), 33471–33484.

Berry, P.A.M., Jasper, A., Bracke, H., 1997. Retracking ERS-1 altimeter waveforms over land for topographic height determination: an expert system approach. Eur. Space Agency Spec. Publ. ESA SP-414, 403–408.

Boy, F., Desjonquères, J.-D., Picot, N., Moreau, T., Raynal, M., 2017. CRYOSAT-2 SAR mode over oceans: processing methods, global assessment and benefits. IEEE Trans. Geosci. Remote Sens. 55, 148–158.

Brown, G.S., 1977. The average impulse response of a rough surface and its applications. IEEE Trans. Antennas Propag. 25, 67–74.

Chen, G., Chapron, B., Ezraty, R., Vandemark, D., 2002. A global view of swell and wind sea climate in the ocean by satellite altimeter and scatterometer. J. Atmos. Oceanic Technol. 19, 1849–1859.

Cotton, D., Naeije, M., Scharroo R., et al., 2015. Cryosat Plus for Oceans: Final Report, Executive Summary and Abstract, Technical Report for ESA, Contract No. 4000106169/12/I-NB.

Dibarboure, G., Boy, F., Desjonqueres, J.-D., Labroue, S., Lasne, Y., Picot, N., Poisson, J.-C., Thibaut, P., 2014. Investigating short wavelength correlated errors on low-resolution mode altimetry. J. Atmos. Ocean Technol. 31 (6), 1337–1362.

Dumont, J.-P., 1985. Estimation Optimale des Paramètres Altimétriques des Signaux Radar Poseidon ("Optimal estimation of altimetric parameters of POSEIDON radar signal), PhD Thesis from Institut National Polytechnique de Toulouse, Toulouse, France.

Durden, S.L., Vesecky, J.F., 1985. A physical radar cross-section model for a wind-driven sea with swell. IEEE J. Oceanic Eng. OE-10, 445–451.

Fenoglio-Marc, L., Dinardo, S., Scharroo, R., Roland, A., Lucas, B., Weiss, R., Dutour Sikirić, M., Becker, M., Benveniste, J., 2015. A Validation exercise for CryoSat-2 in SAR mode in the German Bight Area. Adv. Space Res. 11, 2641–2656.

Gaspar, P., Florens, J.-P., 1998. Estimation of the sea state bias in radar altimeter measurements of sea level: results from a new nonparametric method. J. Geophys. Res. 103 (C8), 15803–15814.

Gaspar, P., Labroue, S., Ogor, F., Lafitte, G., Marchal, L., Rafanel, M., 2002. Improving nonparametric estimates of the sea state bias in radar altimetry measurements of sea level. J. Atmos. Oceanic Technol. 19, 1690–1707.

Gommenginger, C., Martin-Puig, C., Amarouche, L., Raney, R.K., 2013. Jason-CS SAR mode error budget study: review of state of knowledge for SAR altimetry over ocean. Technical Report for EUMETSAT, EUM/RSP/REP/14/749304.

Halimi, A., Mailhes, C., Tourneret, J.Y., Thibaut, P., Boy, F., 2014. A semi-analytical model for delay/Doppler altimetry and its estimation algorithm. IEEE Trans. Geosci. Remote Sens. 52 (7), 4248–4258.

Hayne, G.S., 1980. Radar altimeter mean return waveforms from near-normal incidence ocean surface scattering. IEEE Trans. Antennas Propag. 28, 687–692.

Labroue, S., Gaspar, P., Dorandeu, J., Zanife, O.Z., Mertz, F., Vincent, P., Choquet, D., 2004. Non-parametric estimates of the sea state bias for Jason-1 radar altimeter. Mar. Geod. 27, 453–481.

Legresy, B., Remy, F., 1997. Altimetric observations of surface characteristics of the Antarctic Ice Sheet. J. Glaciol. 43, 265–275.

Raney, R.K., 1998. The delay/Doppler radar altimeter. IEEE Trans. Geosci. Remote Sens. 36, 1578–1588.

Rascle, N., Ardhuin, F., 2013. A global wave parameter database for geophysical applications. Part 2: model validation with improved source term parameterization. Ocean Modell. 70, 174–178.

Ray, C., Martin-Puig, C., Clarizia, M.P., Ruffini, G., Dinardo, S., Gommenginger, C., Benveniste, J., 2015. SAR altimeter backscattered waveform model. IEEE Trans. Geosci. Remote Sens. 53 (2), 911–919.

Raynal, M., Labroue, S., Moreau, T., Boy, F., Picot, N., 2018. From conventional to delay doppler altimetry: a demonstration of continuity and improvements with Cryosat-2 mission. Adv. Space Res. 62 (6), 1564–1575.

Rodriguez, E., 1988. Altimetry for non-Gaussian oceans: height biases and estimation of parameters. J. Geophys. Res. 93, 14107–14120.

Semedo, A., Sušelj, K., Rutgersson, A., Sterl, A., 2011. A Global view on the wind sea and swell climate and variability from ERA-40. J. Climate 24 (5), 1461–1479.

Sterl, A., Caires, S., 2005. Climatology variability and extrema of ocean waves, the web-based NLMI/ERA-40 Wave Atlas. Int. J. Climatol. 25, 963–977. Published online in Wiley InterScience (http://www.interscience.wiley.com).

Thibaut, P., Poisson, J.C., Bronner, E., Picot, N., 2010. Relative performance of the MLE3 and MLE4 retracking algorithms on Jason-2 altimeter waveforms. Mar. Geod. 33 (S1), 317–335.

Tournadre, J., Chapron, B., Reul, N., Vandemark, D.C., 2006. A satellite altimeter model for Ocean slick detection. J. Geophys. Res. 111, C04004.

Tran, N., Labroue, S., Philipps, S., Bronner, E., Picot, N., 2010a. Overview and update of the sea state bias corrections for the Jason-2, Jason-1 and TOPEX missions. Mar. Geod./special issue on OSTM/Jason-2 calibration/validation 33 (S1), 348–362. https://doi.org/10.1080/01490419.2010.487788.

Tran, N., Vandemark, D., Labroue, S., Feng, H., Chapron, B., Tolman, H.L., Lambin, J., Picot, N., 2010b. The sea state bias in altimeter sea level estimates determined by combining wave model and satellite data. J. Geophys. Res. 115, C03020.

Wingham, D.J., Francis, C.R., Baker, S., Bouzinac, C., Brockley, D., Cullen, R., de Chateau-Thierry, P., Laxon, S., Mallow, U., Mavrocordatos, C., Phalippou, L., Ratier, G., Rey, L., Rostan, F., Viau, P., Wallis, D., 2006. Cryosat: a mission to determine the fluctuations in Earth's land and marine ice fields. Adv. Space Res. 37 (4), 841–871.